




Fast numerical algorithm for the reaction-diffusion equations using an interpolating method

Sungha Yoon¹ · Chaeyoung Lee² · Soobin Kwak³ · Seungyoon Kang³ · Junseok Kim³ 

Received: 27 June 2023 / Revised: 4 January 2024 / Accepted: 19 November 2024 /

Published online: 28 November 2024

© The Author(s) under exclusive licence to Sociedade Brasileira de Matemática Aplicada e Computacional 2024

Abstract

We present a fast and splitting-based numerical scheme that employs an interpolation method for the system of the reaction-diffusion equations. Typically, the time step restriction arises to the nonlinear reaction terms when we calculate the highly stiff system of reaction-diffusion equations. This issue can be resolved through various implicit solvers, but they shall present another problem of having a longer computing time for each step. In order to overcome these shortcomings, we present a splitting-based hybrid scheme with a pre-iteration process before the main loop to derive interpolating points which are employed to evaluate the intermediate solution, instead of computing the nonlinear reaction term directly. The stability and convergence analysis are provided for selected reaction-diffusion models. We verify that the results of our proposed method are in good agreements with those in the references, as demonstrated numerically. Furthermore, we examine and compare the computing time performance among the methods, and draw that our proposed method yields good results.

Keywords Interpolating · Splitting method · Reaction-diffusion equations

Mathematics Subject Classification 35K57 · 65M12 · 65M20

✉ Junseok Kim
cfdkim@korea.ac.kr

Sungha Yoon
there122@ewha.ac.kr

Chaeyoung Lee
cylee@kyonggi.ac.kr

Soobin Kwak
soobin23@korea.ac.kr

Seungyoon Kang
heroe2401@korea.ac.kr

¹ Institute of Mathematical Sciences, Ewha Womans University, Seoul 30019, Republic of Korea

² Department of Mathematics, Kyonggi University, Suwon 16227, Republic of Korea

³ Department of Mathematics, Korea University, Seoul 02841, Republic of Korea

1 Introduction

Patterns of alive creatures, especially focused on such as shellfish, mammals, had been widely investigated due to importance of their morphogenesis (Lyons and Harrison 1992; Ermentrout 1991). Despite many of previous studies, it is not yet clear how genetic patterns of skin in mammals and other organisms are made. Therefore, various models are worth studying, of which one of the mathematical models is the reaction-diffusion type model. This model is proposed earlier by Turing (1990), which can autonomously generate several spatial patterns. Further researches are conducted to verify the role of reaction-diffusion system for spatial pattern formation in mathematical biology (Kondo and Miura 2010; Othmer and Pate 1980; Greenberg et al. 1978). Barrio et al. (1999) extended the previous studies of Turing systems to investigate the characteristics of domain influence, nonlinearity, and boundary conditions for both coupled reaction-diffusion equations and coupled interacting systems. The authors presented admissible modes for the corresponding model to specify the patterns and carried out detailed numerical simulation results which are concerned with skin patterns of fish, kinds of dotted or striped, which are derived from the diffusion-driven instability. Lengyel and Epstein (1992) derived mathematical models to design chemical systems. The patterns that the model predicts are in good agreement with the experimental results.

Sherratt et al. (2002) presented the cyclic predator–prey interaction which is prey ratio dependent functional response with diffusion. This model is followed from the Turing instabilities, and has a family of traveling waves (Dunbar 1986) which has induced by landscape features with specific boundary conditions. With only homogeneous Neumann boundary conditions, solution waves quickly becomes to uniform oscillations; while waves develop into circular and spiral behaviors with additional zero-density conditions around the obstacle. Furthermore, the authors found that the irregularities of waves are generated moving away from the obstacle since the asymptotic solution is unstable. On the one hand, they represented the corresponding system using a coupled map lattice model instead of a reaction-diffusion system since the populations in domain are not continuous but discrete with interconnected patches. This approach made it possible to implement more complex behaviors of wave solutions. As a follow-up study, Yun et al. (2015) investigated numerically periodic traveling wave solutions with the model in Sherratt et al. (2002), especially focused on shape of both domain and obstacle. They use a complex multigrid solver to compute the numerical solutions. Such model can be applied to other various areas such as kinetic model of a binary mixture undergoing reversible and irreversible chemical reactions (Bisi and Travaglini 2022).

The development of methodologies for numerically solving the models mentioned above has been an important subject of research for a long time. There are several previous research to propose fast and efficient numerical solvers for some stiff equations (Fuselier and Wright 2013; Zhu et al. 2009; Roul and Goura 2019; Roul 2020; Roul and Goura 2022). As can be understood from the contents of these references, the computing cost of most nonlinear reaction terms is considerable when solving various kinds of reaction-diffusion systems. Several cases can be considered: First, if the classical explicit method is used to this system then it usually has a severe time step restriction in reaction terms, especially for large-scale problems. Second, the issue of time step restriction is relaxed when fully implicit or nonlinear semi-implicit schemes are employed, but the computing time per one-step becomes longer inevitably. Third, if we treat the nonlinear terms explicitly while the linear terms implicitly, this linear semi-implicit scheme leads to a better computing time performance than the second one but still have a degraded performance in stiff problems.

In the same vein as the direction pursued by previous studies, one way to achieve fast computation is by using splitting and interpolating. Splitting the system of reaction-diffusion equations leads to solving both systems of ordinary differential equations and diffusion equations sequentially. An important idea is to create interpolating points by pre-computing the system of ordinary differential equations with a determined short-time temporal step before the main time loop. In a nutshell, the primary purpose of this paper is to propose a fast computing algorithm for a system of reaction-diffusion equations using the bilinear interpolation method with a pre-computed solution field.

The paper is organized as follows. In Sect. 2, we propose a hybrid algorithm to compute the numerical solutions for the reaction-diffusion equations. We perform the stability and convergence analysis of our method for selected numerical models in Sect. 3. The numerical simulation results are presented in Sect. 4. Further discussions are addressed in Sect. 5. We end up this paper with conclusions in Sect. 6.

2 Proposed numerical solution algorithm

In this section, we demonstrate our proposed method which is designed to find numerical solutions of reaction-diffusion equations. Since most pattern formation simulations are performed in the two-dimensional (2D) space, we present the algorithm for the system of equations with two variables in 2D space. Let $\Omega = (a, b) \times (c, d)$ be a spatial domain. The basic form of system of reaction-diffusion equations is as follows (Turing 1990):

$$\frac{\partial u}{\partial t} = F(u, v) + D_u \Delta u, \quad \frac{\partial v}{\partial t} = G(u, v) + D_v \Delta v, \quad (1)$$

where F and G are nonlinear reaction terms, D_u and D_v are diffusion coefficients corresponding to each variable $u \in \Omega \times [0, T]$ and $v \in \Omega \times [0, T]$, respectively. Note that T represents a final time. A formal splitting method breaks (1) into two parts; the first one is the reaction system,

$$\frac{\partial u}{\partial t} = F(u, v), \quad \frac{\partial v}{\partial t} = G(u, v), \quad (2)$$

and the other is the diffusion system,

$$\frac{\partial u}{\partial t} = D_u \Delta u, \quad \frac{\partial v}{\partial t} = D_v \Delta v. \quad (3)$$

Therefore, the solution of the system (1) is derived in time in two substeps as

$$u((n+1)\Delta t) = \mathcal{L}^u(\Delta t) \mathcal{N}^u(\Delta t) u(n\Delta t), \quad v((n+1)\Delta t) = \mathcal{L}^v(\Delta t) \mathcal{N}^v(\Delta t) v(n\Delta t), \quad (4)$$

where $\mathcal{N}^u(\Delta t)$ and $\mathcal{N}^v(\Delta t)$ are exact nonlinear solution operators of the system (2) for u and v , respectively, and $\mathcal{L}^u(\Delta t)$ and $\mathcal{L}^v(\Delta t)$ are exact linear solution operators of the system (3) for u and v , respectively.

Because (2) is the system of ordinary differential equations, numerical solutions of (2) can be represented by u and v with respect to t only. The key point is to numerically compute (2) in short-time Δt , which is a discretized time step, before the main loop and to make interpolating points in advance to solve (1) in the main time loop. We employ these interpolating points to create interpolants, which are used to resolve the nonlinear terms in (1).

We discretize the domain Ω to a cell-centered computational domain $\Omega_h = \{(x_i, y_j) = (a + (i - 0.5)h, c + (j - 0.5)h) \mid 1 \leq i \leq N_x, 1 \leq j \leq N_y\}$ where N_x and N_y are the

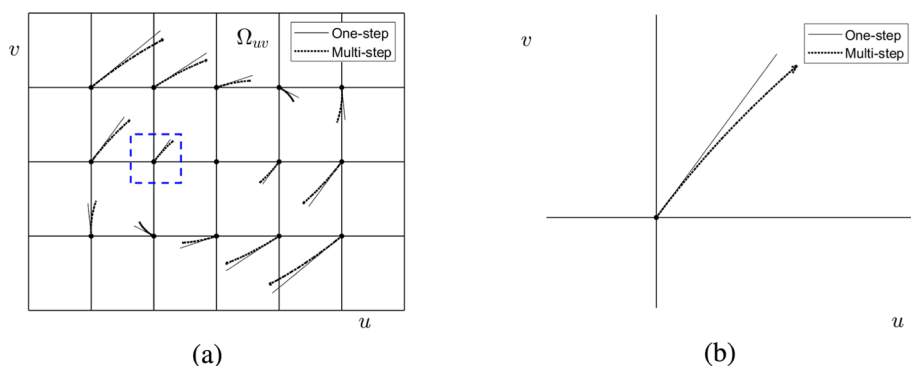


Fig. 1 **a** Illustration of the difference between one-step and multi-step processes in the domain Ω_{uv} . **b** Close up view of blue boxed region in **a**. Note that we use $\Delta t_s = 0.1/10$ in this case for a simplicity of schematic description

number of grid points in x and y directions respectively, and $h = (b-a)/N_x = (d-c)/N_y$ is the uniform spatial step size. Now we describe the pre-computing process which is to solve (2) in advance before the main cycle. Let N_s be the number of pre-iterations and $\Omega_{uv} = [u_{\min}, u_{\max}] \times [v_{\min}, v_{\max}]$ be a uv -domain. We employ the new parameters N_u and N_v , the number of sample points in each axis u and v respectively. A discretized uv -domain is defined as $\Omega_H = \{(u_p, v_q) = (u_{\min} + (p-1)H, v_{\min} + (q-1)H) \mid 1 \leq p \leq N_u, 1 \leq q \leq N_v\}$, where $H = (u_{\max} - u_{\min})/(N_u - 1) = (v_{\max} - v_{\min})/(N_v - 1)$ is a uniform grid step size. We discretize (2) using the classical explicit fourth-order Runge–Kutta method as follows: For $1 \leq p \leq N_u$ and $1 \leq q \leq N_v$,

$$\begin{aligned} \frac{u_{\{p,q\}}^{m+1} - u_{\{p,q\}}^m}{\Delta t_s} &= \frac{1}{6}(\alpha_1 + 2\alpha_2 + 2\alpha_3 + \alpha_4), \\ \frac{v_{\{p,q\}}^{m+1} - v_{\{p,q\}}^m}{\Delta t_s} &= \frac{1}{6}(\beta_1 + 2\beta_2 + 2\beta_3 + \beta_4), \end{aligned} \quad (5)$$

where $\Delta t_s = \Delta t/N_s$ and α_k, β_k ($k = 1, 2, 3, 4$) are defined as

$$\begin{aligned} \alpha_1 &= F(u_{\{p,q\}}^m, v_{\{p,q\}}^m), \quad \beta_1 = G(u_{\{p,q\}}^m, v_{\{p,q\}}^m), \\ \alpha_2 &= F(u_{\{p,q\}}^m + 0.5\Delta t_s \alpha_1, v_{\{p,q\}}^m + 0.5\Delta t_s \beta_1), \\ \beta_2 &= G(u_{\{p,q\}}^m + 0.5\Delta t_s \alpha_1, v_{\{p,q\}}^m + 0.5\Delta t_s \beta_1), \\ \alpha_3 &= F(u_{\{p,q\}}^m + 0.5\Delta t_s \alpha_2, v_{\{p,q\}}^m + 0.5\Delta t_s \beta_2), \\ \beta_3 &= G(u_{\{p,q\}}^m + 0.5\Delta t_s \alpha_2, v_{\{p,q\}}^m + 0.5\Delta t_s \beta_2), \\ \alpha_4 &= F(u_{\{p,q\}}^m + \Delta t_s \alpha_3, v_{\{p,q\}}^m + \Delta t_s \beta_3), \\ \beta_4 &= G(u_{\{p,q\}}^m + \Delta t_s \alpha_3, v_{\{p,q\}}^m + \Delta t_s \beta_3). \end{aligned}$$

Using the above multi-step process for Δt , i.e., using Δt_s is essential because it provides more accurate results than the one-step ($N_s = 1$) process for Δt . Figure 1 depicts the difference between one-step and multi-step processes.

Note that we have discretized (5) with respect to not only time but also uv -space since we have to generate interpolating points to make interpolants for solving (2) in uv -space. After that we can obtain the intermediate solutions (u^*, v^*) of (1) in xy -space. We compute (5) for

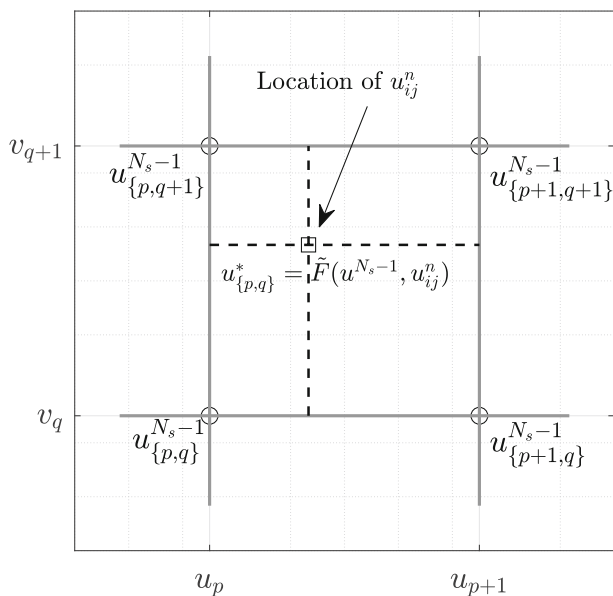


Fig. 2 Schematic illustration of the bilinear interpolation process in a specific cell where u_{ij}^n is located. Note that an input value u_{ij}^n in Ω_h is transferred to Ω_H in the grid order of Ω_h

$m = 0, \dots, N_s - 1$ with $u_{p,q}^0 = u_p$ and $v_{p,q}^0 = v_q$. We call the interpolating functions $\tilde{F}(u^{N_s-1}, \bullet)$ and $\tilde{G}(v^{N_s-1}, \bullet)$ in u - and v -direction, respectively, in uv -space. Where \bullet is indicated, u_{ij}^n and v_{ij}^n in xy -space are assigned to \tilde{F} and \tilde{G} , respectively, in grid order. Thus, u_{ij}^n and v_{ij}^n must exist inside a certain cell of Ω_H ; hence these points become query points and then the bilinear interpolation is adopted to both interpolating functions. Accordingly, we have a numerical solution $(u_{p,q}^*, v_{p,q}^*)$ in uv -space and pull back to (u_{ij}^*, v_{ij}^*) in xy -space, therefore, it can be written as

$$(u_{ij}^*, v_{ij}^*)_{\Omega_h} = \left(\tilde{F}(u^{N_s-1}, u_{ij}^n), \tilde{G}(v^{N_s-1}, v_{ij}^n) \right)_{\Omega_H}. \quad (6)$$

Figure 2 depicts the bilinear interpolation process in a specific cell where u_{ij}^n is located.

Then, we employ the intermediate solution to solve the diffusion system (3). The following implicit Fourier-spectral method is applied to solving (3) if the periodic boundary condition is given. For the given data $\{(u_{ij}^*, v_{ij}^*) \mid 1 \leq i \leq N_x, 1 \leq j \leq N_y\}$, the discrete Fourier transform is defined as

$$\hat{u}_{rs}^* = \sum_{i=1}^{N_x} \sum_{j=1}^{N_y} u_{ij}^* e^{-i(\xi_r x_i + \eta_s y_j)}, \quad \hat{v}_{rs}^* = \sum_{i=1}^{N_x} \sum_{j=1}^{N_y} v_{ij}^* e^{-i(\xi_r x_i + \eta_s y_j)},$$

where $\xi_r = 2\pi r/(b-a)$ and $\eta_s = 2\pi s/(d-c)$. The corresponding solver is as follows:

$$\hat{u}_{rs}^{n+1} = \frac{\hat{u}_{rs}^*}{1 + \Delta t(\xi_r^2 + \eta_s^2)}, \quad \hat{v}_{rs}^{n+1} = \frac{\hat{v}_{rs}^*}{1 + \Delta t(\xi_r^2 + \eta_s^2)}. \quad (7)$$

Lastly, we employ the inverse discrete Fourier transform as

$$u_{ij}^{n+1} = \frac{1}{N_x N_y} \sum_{r=-N_x/2+1}^{N_x/2} \sum_{s=-N_y/2+1}^{N_y/2} \hat{u}_{rs}^{n+1} e^{i(\xi_r x_i + \eta_s y_j)},$$

$$v_{ij}^{n+1} = \frac{1}{N_x N_y} \sum_{r=-N_x/2+1}^{N_x/2} \sum_{s=-N_y/2+1}^{N_y/2} \hat{v}_{rs}^{n+1} e^{i(\xi_r x_i + \eta_s y_j)}.$$

Diffusion terms are solved using the following explicit scheme if other boundary conditions are given.

$$u_{ij}^{n+1} = u_{ij}^* + \Delta t \left(\frac{u_{i-1,j}^* + u_{i+1,j}^* + u_{i,j-1}^* + u_{i,j+1}^* - 4u_{ij}^*}{h^2} \right),$$

$$v_{ij}^{n+1} = v_{ij}^* + \Delta t \left(\frac{v_{i-1,j}^* + v_{i+1,j}^* + v_{i,j-1}^* + v_{i,j+1}^* - 4v_{ij}^*}{h^2} \right). \quad (8)$$

Now we can express (4) using numerical solution operators as follows:

$$u^{n+1} = \mathcal{L}_h^u(\Delta t) \mathcal{N}_h^u(\Delta t) u^n, \quad v^{n+1} = \mathcal{L}_h^v(\Delta t) \mathcal{N}_h^v(\Delta t) v^n,$$

where $N_h^u(\Delta t) : a_0 \rightarrow \tilde{F}(u^{N_s-1}, a_0)$ and $N_h^v(\Delta t) : b_0 \rightarrow \tilde{G}(u^{N_s-1}, b_0)$ are discrete nonlinear solution operators, as defined in (6), for each initial input a_0 and b_0 at each time level. $L_h^u(\Delta t)$ and $L_h^v(\Delta t)$ are discrete linear solution operators and these follow (7) if the periodic boundary condition is adopted, and (8) if other boundary conditions are given. The following Algorithm 1 is a summary of the entire process.

Algorithm 1 Hybrid splitting-based scheme using interpolants

Require: the split systems (2) and (3)

1. Initialize u and v as (u^0, v^0)
 2. Solve the system (2) using the explicit Runge–Kutta method to generate the interpolating points
 3. Update the intermediate solutions u^* and v^* via bilinear interpolation (6)
 4. Solve the system (3) as follows
 - if** the periodic boundary condition is given **then**
 - Update u^{n+1} and v^{n+1} via implicit solver (7)
 - else**
 - Update u^{n+1} and v^{n+1} via explicit solver (8)
 - end if**
 5. If the final time is reached **STOP** else **GOTO** 3
-

Remark 1 The above splitting scheme is called the Lie–Trotter splitting method (Trotter 1959), and sometimes also called the first order Strang splitting scheme. This scheme for a partial differential equation with variable w has two features as follows:

$$\mathcal{O}(\Delta t^2) \text{ local error per one-step } \Delta t : \|\mathcal{L}(\Delta t) \mathcal{N}(\Delta t) w^n - w^{n+1}\| = \mathcal{O}(\Delta t^2), \quad (9)$$

$$\mathcal{O}(\Delta t) \text{ global error in } -\mathcal{O}(1)\text{-time } t \leq T : \sup_{t \leq T} \|\mathcal{L}(t) \mathcal{N}(t) w^0 - w^n\| = \mathcal{O}(\Delta t), \quad (10)$$

where $\|\cdot\|$ is some Sobolev norm and $w^0 \in H^k(\Omega)$ for some $k \geq 1$. However, we will not discuss higher-order Sobolev bounds for our method in this paper.

Remark 2 Since we compute the nonlinear part using the bilinear interpolation with pre-computed interpolating points, in the sense of fully explicit formula, there is no need for a certain coefficient matrix to solve the system (6). Furthermore, the fully explicit solver (8) is used unless the periodic boundary condition is adopted; this is the same case as earlier. Therefore, only the stability condition for (7) has been considered. For simplicity, define the discrete Fourier space as $\Omega_F = [-k_{max}, k_{max}]^2$ where $k_{max} = 2\pi(N/2 - 1)/L$ with $L = b - a = d - c$ and $N = N_x = N_y$ is even. Let the grid points be gathered into a vector with a lexicographic order of the nodes in Ω_F . Now define a solution vector as $U^n \in \mathbb{C}^{N^2}$ at $t = n\Delta t$, then we have

$$(I - \Delta t A_h)U^{n+1} = U^n,$$

where A_h is the ordered discrete Laplacian matrix. Note that A_h is purely diagonal from (7). Clearly, A_h has two simple eigenvalues, the smallest and the largest, and the others are

$$\lambda_{rs} = -\frac{4}{h^2} \left(\sin^2 \left(\frac{(r-1)\pi}{2N} \right) + \sin^2 \left(\frac{(s-1)\pi}{2N} \right) \right),$$

for $1 \leq r, s \leq N/2 - 2$ with multiplicities 2. Since the smallest one is zero, the smallest eigenvalue of the update matrix is one. The largest one is scaled by the square of $(N/2 - 1)$, which is the wave number of the corresponding eigenvector; so the condition number of A_h is $\mathcal{O}(N^2)$. Simply we estimate the spectral norm of the update matrix as

$$\|I - \Delta t A_h\|_t \leq 1 + \Delta t \|A_h\|_t,$$

where $\|\cdot\|_t$ is the spectral norm of a matrix. Therefore, the condition number of the update matrix is $\mathcal{O}(N^2)$ since the spectral norm of the symmetric matrix equals its largest eigenvalue. Instead of adjusting the condition through the preconditioning, we adopt $\Delta t = \mathcal{O}(h^2)$ (or $\mathcal{O}(h)$ if N is not quite large) for $h = L/N < 1$. Then the condition number of the update matrix is nearly optimal, $\mathcal{O}(1)$.

3 Numerical analysis

We examine the stability and convergence of our method applied to two reaction-diffusion models (Lengyel and Epstein 1992; Sherratt et al. 2002) theoretically in this section. Previous to introduce the models, we define the following discrete norms in 2D.

$$\|w\|_{2,\Omega_h} = \left(h^2 \sum_{i,j} w_{ij}^2 \right)^{1/2}, \quad \|w\|_{\infty,\Omega_h} = \max_{i,j} \{w_{ij}\}. \quad (11)$$

The space subscript is omitted only for Ω_h in (11) hereafter.

3.1 Lengyel–Epstein model

First, we introduce the model in Lengyel and Epstein (1992) as follows:

$$\frac{\partial u}{\partial t} = k_1 \left(v - \frac{uv}{1+v^2} \right) + \Delta u, \quad \frac{\partial v}{\partial t} = k_2 - v - \frac{4uv}{1+v^2} + \delta \Delta v, \quad (12)$$

where u is an inhibitor and v is an activator, and k_1 and k_2 are positive constants, and $\delta \leq 1$ is a ratio of diffusion coefficients. Note that this system has a linearly stable steady-state solution $(1 + (0.2k_2)^2, 0.2k_2)$. The periodic boundary condition is employed.

First, we show the following stability result.

Theorem 1 Suppose that $\Delta t \leq \min\{1, \frac{1+k_2^2}{k_1k_2}\}$, and $1 + \epsilon^2 < u_{ij}^0 < 1 + k_2^2$, and $\epsilon < v_{ij}^0 < k_2$ where $\epsilon = k_2/(5 + 4k_2^2)$ for all $1 \leq i \leq N_x$ and $1 \leq j \leq N_y$. Then we have

$$\|u^{n+1}\|_2 < 1 + k_2^2, \quad \|v^{n+1}\|_2 < k_2.$$

Proof Since $u^{n+1} = \mathcal{L}_h^u(\Delta t)\mathcal{N}_h^u(\Delta t)u^n$ and $v^{n+1} = \mathcal{L}_h^v(\Delta t)\mathcal{N}_h^v(\Delta t)v^n$, we begin the proof by finding upper bounds for the nonlinear reaction systems, one for u and the other for v , respectively. As described in Sect. 2, once we have u_{ij}^n and v_{ij}^n , these must be located in the certain cells in Ω_H . Now we define the maximum values of each certain cell as $u_{ij}^{*,max} = \max\{u_{\{p_1,q_1\}}^{N_s-1}, u_{\{p_1+1,q_1\}}^{N_s-1}, u_{\{p_1,q_1+1\}}^{N_s-1}, u_{\{p_1+1,q_1+1\}}^{N_s-1}\}$ and $v_{ij}^{*,max} = \max\{v_{\{p_2,q_2\}}^{N_s-1}, v_{\{p_2+1,q_2\}}^{N_s-1}, v_{\{p_2,q_2+1\}}^{N_s-1}, v_{\{p_2+1,q_2+1\}}^{N_s-1}\}$, respectively. Due to the nature of the bilinear interpolation, we have

$$\mathcal{N}_h^u(\Delta t)u_{ij}^n = u_{ij}^* \leq u_{ij}^{*,max}, \quad \mathcal{N}_h^v(\Delta t)v_{ij}^n = v_{ij}^* \leq v_{ij}^{*,max},$$

for all $1 \leq i \leq N_x$ and $1 \leq j \leq N_y$. Now we use the following useful a priori estimates of the system (12) to get upper bounds of $\|u^{*,max}\|_{\infty,\Omega_H}$ and $\|v^{*,max}\|_{\infty,\Omega_H}$, respectively. We start first with v as

$$k_2 - v - \frac{4uv}{1+v^2} < k_2 - v. \quad (13)$$

Using the well-known comparison theorem in Smoller (2012), we can conclude that $v(\cdot, t) < k_2$ for all $t > 0$. Furthermore, based on the maximum principle argument for parabolic problems and (Yi et al. 2009), we have

$$u \leq \frac{v(1+v^2)}{4v} < 1 + k_2^2, \quad (14)$$

in the linearly stable region $(u, v) \in (0, 1 + k_2^2) \times (0, k_2)$. Thus, $u(\cdot, t) < 1 + k_2^2$ for all $t > 0$. We omit the proof of deriving lower bounds of each u and v for the sake of clarity. For further details, readers are referred to Yi et al. (2009), Lou and Ni (1996), and the references therein. From (13) and (14), we have $\Delta t \leq \min\{1, \frac{1+k_2^2}{k_1k_2}\}$ for the bounds of the pre-computed interpolating points to be valid. Therefore, the boundedness of both $\|u^{*,max}\|_{\infty,\Omega_H}$ and $\|v^{*,max}\|_{\infty,\Omega_H}$ is also valid, i.e., $\|u^*\|_{\infty} < 1 + k_2^2$ and $\|v^*\|_{\infty} < k_2$.

For the next step, we proceed the proof of finding bounds for the linear diffusion systems. Using the Parseval's identity and $\xi_r^2 + \eta_s^2 > 0$ for all $-N_x/2 + 1 \leq r \leq N_x/2$ and $-N_y/2 + 1 \leq s \leq N_y/2$, we have the following from the implicit solver (7).

$$\begin{aligned} \|u^{n+1}\|_2 &= \sqrt{\frac{1}{N_x N_y} \sum_{r,s} |\hat{u}_{rs}^{n+1}|^2} \leq \sqrt{\frac{1}{N_x N_y} \sum_{r,s} |\hat{u}_{rs}^*|^2} = \|u^*\|_2 < 1 + k_2^2, \\ \|v^{n+1}\|_2 &= \sqrt{\frac{1}{N_x N_y} \sum_{r,s} |\hat{v}_{rs}^{n+1}|^2} \leq \sqrt{\frac{1}{N_x N_y} \sum_{r,s} |\hat{v}_{rs}^*|^2} = \|v^*\|_2 < k_2, \end{aligned}$$

for all $\Delta t > 0$. This completes the proof.

Before showing the convergence result of our method, we define a sample operator and address several lemmas based on Li et al. (2017). Note that the consistency of the numerical solution operator $\mathcal{L}_h(\Delta t)\mathcal{N}_h(\Delta t)$ to the exact solution operator $\mathcal{L}(\Delta t)\mathcal{N}(\Delta t)$ has been proved in various earlier works (Li et al. 2022; Jia and Li 2011). Hence, we omit the proof for convenience; for further details, readers are referred to Li et al. (2022), Jia and Li (2011) and the references therein. Consider the following sample operator $I^h : C^0(\Omega) \rightarrow \mathbb{R}^{N_x \times N_y}$ as $I^h w = \{(w(x_i, y_j))_{ij}\}$. For simplicity, we define the following with respect only u . Therefore, v can be defined in the same way; hence, it will be omitted. Let \tilde{u} be the exact solution of the scheme (4). Therefore, we have $I^h u(n\Delta t) = U^n$ and $I^h \tilde{u}(n\Delta t) = \tilde{U}^n$. Write $U^n_{ij} = u(x_i, y_j, n\Delta t)$ and $\tilde{U}^n_{ij} = \tilde{u}(x_i, y_j, n\Delta t)$, and define u^n_{ij} is a fully discretized numerical approximation of \tilde{U}^n_{ij} . Now we present the following lemmas to discuss the convergence result.

Lemma 1 Assume that $\Delta t \leq \min\{1, \frac{1+k_2^2}{k_1 k_2}\}$. Then

$$\|\mathcal{N}_h^u(\Delta t)\tilde{U}\|_2 \leq e^{\Delta t} \|\tilde{U}\|_2, \quad \|\mathcal{N}_h^v(\Delta t)\tilde{V}\|_2 \leq e^{\Delta t} \|\tilde{V}\|_2,$$

for any $\tilde{U}, \tilde{V} \in \mathbb{R}^{N_x \times N_y}$ satisfying $\|\tilde{U}\|_2 < 1 + k_2^2$, and $\|\tilde{V}\|_2 < k_2$.

Proof This result is directly derived from Theorem 1.

Lemma 2 For any $\Delta t > 0$, we have

$$\|\mathcal{L}_h^u(\Delta t)\tilde{U}\|_2 \leq \|\tilde{U}\|_2, \quad \|\mathcal{L}_h^v(\Delta t)\tilde{V}\|_2 \leq \|\tilde{V}\|_2,$$

for any $\tilde{U}, \tilde{V} \in \mathbb{R}^{N_x \times N_y}$ satisfying $\|\tilde{U}\|_2 < 1 + k_2^2$, and $\|\tilde{V}\|_2 < k_2$.

Proof This result is also directly derived from Theorem 1.

From now on, we denote C , which may or may not include a subscript, as a positive constant can change its value in different contexts.

Lemma 3 (Li et al. 2017) Assume that $u, v \in H^6(0, T; H^3(\Omega))$. Then we have

$$\begin{aligned} \|I^h \mathcal{N}^u(\Delta t)u - \mathcal{N}_h^u(\Delta t)I^h u\|_2 &\leq C_1 \Delta t^5, \\ \|I^h \mathcal{N}^v(\Delta t)v - \mathcal{N}_h^v(\Delta t)I^h v\|_2 &\leq C_2 \Delta t^5, \end{aligned}$$

where C_1 and C_2 are independent on Δt and h .

Proof The proof is similar that is given in Li et al. (2017). Therefore, we omit the proof here for convenience.

Lemma 4 (Li et al. 2017) Assume that $u, v \in H^3(0, T; H^k(\Omega))$ for some $k \geq 2$. Then there are C_1 and C_2 independent on Δt and h such that

$$\begin{aligned} \|I^h \mathcal{L}^u(\Delta t)u - \mathcal{L}_h^u(\Delta t)I^h u\|_2 &\leq C_1 |u|_k e^{\Delta t} h^k, \\ \|I^h \mathcal{L}^v(\Delta t)v - \mathcal{L}_h^v(\Delta t)I^h v\|_2 &\leq C_2 |v|_k e^{\Delta t} h^k, \end{aligned}$$

where $|u|_k = \left(\sum_{r,s} (\xi_r^2 + \eta_s^2)^k |\hat{u}_{rs}|^2 \right)^{1/2}$ and $|v|_k = \left(\sum_{r,s} (\xi_r^2 + \eta_s^2)^k |\hat{v}_{rs}|^2 \right)^{1/2}$ are the seminorms in $H^k(\Omega)$.

Proof The proof is given in Li et al. (2017). Hence, we omit the proof for simplicity.

The convergence of our proposed method is shown by the following theorem. This result is based on the framework in Li et al. (2017).

Theorem 2 We set $I^h u^0 = U^0 = u^0$ and $I^h v^0 = V^0 = v^0$, and let u^0 and v^0 be given as in Theorem 1. Suppose that $\Delta t \leq \min\{1, \frac{1+k_2^2}{k_1 k_2}\}$ and $u^0, v^0 \in H^k(\Omega)$ for some $k \geq 4$. Furthermore, assume that $u, v \in H^6(0, T; H^k(\Omega))$ are the exact solutions of the system (12). Let $U^{n+1} = I^h u((n+1)\Delta t)$, $V^{n+1} = I^h v((n+1)\Delta t)$ be the solutions assigned at all the grid points. Then there are C_1 and C_2 independent on Δt and h satisfying

$$\begin{aligned}\|U^{n+1} - u^{n+1}\|_2 &\leq C_1 \left(\Delta t + \frac{h^k}{\Delta t} \right), \\ \|V^{n+1} - v^{n+1}\|_2 &\leq C_2 \left(\Delta t + \frac{h^k}{\Delta t} \right).\end{aligned}$$

If we take $\Delta t = \mathcal{O}(h^2)$, then we have

$$\begin{aligned}\|U^{n+1} - u^{n+1}\|_2 &\leq C_1 \Delta t, \\ \|V^{n+1} - v^{n+1}\|_2 &\leq C_2 \Delta t.\end{aligned}$$

Proof For the sake of clarity, we show the case of u only. Suppose that the n -th numerical solution u^n is given. Now we apply the one-step exact solution operator $\mathcal{L}^u(\Delta t)\mathcal{N}^u(\Delta t)$ to \tilde{u}^n , which is the n -th exact solution of (4), and denote it as $\tilde{U}^{n+1} = I^h \mathcal{L}^u(\Delta t)\mathcal{N}^u(\Delta t)\tilde{u}^n$. Then we have

$$\|U^{n+1} - u^{n+1}\|_2 \leq \|U^{n+1} - \tilde{U}^{n+1}\|_2 + \|\tilde{U}^{n+1} - u^{n+1}\|_2. \quad (15)$$

From (9), the first term on the right-hand side of (15) is the local one-step error (9); hence, it follows that

$$\|U^{n+1} - \tilde{U}^{n+1}\|_2 \leq C_1 \Delta t^2.$$

The second term on the right-hand side of (15) is

$$\begin{aligned}\|\tilde{U}^{n+1} - u^{n+1}\|_2 &\leq \|I^h \mathcal{L}^u(\Delta t)\mathcal{N}^u(\Delta t)\tilde{u}^n - \mathcal{L}_h^u(\Delta t)I^h \mathcal{N}^u(\Delta t)\tilde{u}^n\|_2 \\ &\quad + \|\mathcal{L}_h^u(\Delta t)I^h \mathcal{N}^u(\Delta t)\tilde{u}^n - \mathcal{L}_h^u(\Delta t)\mathcal{N}_h^u(\Delta t)u^n\|_2.\end{aligned} \quad (16)$$

Using Lemmas 2 and 4, then the right-hand side of (16) is bounded by

$$C_2 |\mathcal{N}^u(\Delta t)\tilde{u}^n|_k e^{\Delta t} h^k + \|I^h \mathcal{N}^u(\Delta t)\tilde{u}^n - \mathcal{N}_h^u(\Delta t)u^n\|_2. \quad (17)$$

The second term in (17) is bounded by

$$\|I^h \mathcal{N}^u(\Delta t)\tilde{u}^n - \mathcal{N}_h^u(\Delta t)I^h \tilde{u}^n\|_2 + \|\mathcal{N}_h^u(\Delta t)I^h \tilde{u}^n - \mathcal{N}_h^u(\Delta t)u^n\|_2. \quad (18)$$

Using Lemmas 1 and 3, (18) is bounded by

$$C_3 \Delta t^5 + e^{\Delta t} \|I^h \tilde{u}^n - u^n\|_2 = C_3 \Delta t^5 + e^{\Delta t} \|\tilde{U}^n - u^n\|_2.$$

Combining all above estimates yields

$$\begin{aligned}\|U^{n+1} - u^{n+1}\|_2 &\leq C_1 \Delta t^2 + C_2 |\mathcal{N}^u(\Delta t)\tilde{u}^n|_k e^{\Delta t} h^k + C_3 \Delta t^5 + e^{\Delta t} \|\tilde{U}^n - u^n\|_2 \\ &\leq (n+1) \left(C_1 \Delta t^2 + C_2 h^k \max_{0 \leq s \leq n} \{|\mathcal{N}^u(\Delta t)\tilde{u}^s|_k\} \right) + e^{2T} \|\tilde{U}^0 - u^0\|_2\end{aligned}$$

$$= C \left(\Delta t + \frac{h^k}{\Delta t} \right).$$

If we have $\Delta t = Ch^2$, then

$$\begin{aligned} \|U^{n+1} - u^{n+1}\|_2 &\leq C_1 \left(\Delta t + \frac{h^k}{\Delta t} \right) \leq C_1 \left(\Delta t + C_2 h^{k-2} \right) \\ &\leq C_1 \left(\Delta t + C_2 \Delta t^{k/2-1} \right) = C \Delta t, \end{aligned}$$

since $k \geq 4$. The convergence of v can be analyzed in the same manner. Note that $1 \leq e^{s\Delta t} \leq e^{sT} \leq C$ for any finite s and $\Delta t > 0$; hence, it is absorbed into C . Moreover, C is clearly independent to Δt because we have the upper bound of Δt in the assumption in Theorem 2. This completes the proof.

3.2 Predator–prey model

For the next step, we investigate the predator–prey model which is listed in Sherratt et al. (2002) as follows:

$$\begin{aligned} \frac{\partial u}{\partial t} &= u(1-u) - \frac{\gamma uv}{1+\gamma u} + \Delta u, \\ \frac{\partial v}{\partial t} &= \frac{\gamma uv}{\beta(1+\gamma u)} - \frac{v}{\alpha\beta} + \sigma \Delta v, \end{aligned} \quad (19)$$

where u is a prey and v is a predator, and $\sigma \geq 1$ is a ratio of diffusion coefficients, and α , β , and γ are model coefficients. Note that this system has at least one non-fixed equilibrium node defined as $(\bar{u}, \bar{v}) = (1/(\gamma(\alpha-1)), (1-\bar{u})(1+\gamma\bar{u})/\gamma)$ where $\alpha > 1$. We take the homogeneous Neumann boundary condition.

Now we prove the following stability statement.

Theorem 3 Assume that $\Delta t \leq \min\{1/\sigma, h^2/4\}$, and $\|u^0\|_\infty < 1$, and $\|u^0\|_\infty < \|v^0\|_\infty < \alpha + \frac{1}{\beta\sigma}$. Then we have

$$\|u^{n+1}\|_\infty < 1, \quad \|v^{n+1}\|_\infty < \alpha + \frac{1}{\beta\sigma}.$$

Proof Define $u_{ij}^{*,max}$ and $v^{*,max}$ in a manner similar to that in the proof of Theorem 1. Then, due to the nature of the bilinear interpolation, the first formula of the method is clearly bounded by

$$\begin{aligned} \mathcal{N}_h^u(\Delta t)u_{ij}^n &= u_{ij}^* \leq u^{*,max} < 1, \\ \mathcal{N}_h^v(\Delta t)v_{ij}^n &= v_{ij}^* \leq v^{*,max} < \alpha + \frac{1}{\beta\sigma}, \end{aligned} \quad (20)$$

for all $1 \leq i \leq N_x$ and $1 \leq j \leq N_y$ if the second inequality in each line of (20) holds. This fact can be derived from the following useful a priori estimates of the system (19). We begin first with u as

$$u(1-u) - \frac{\gamma uv}{1+\gamma u} \leq u(1-u). \quad (21)$$

Using the comparison argument again, we can conclude $0 < u(\cdot, t) < 1$ for all $t > 0$ if $0 < u(\cdot, 0) < 1$. To proceed with the process of obtaining the bound for v , multiply $1/(\beta\sigma)$

to the first equation and divide the second equation by σ in (19), and add the two equations then

$$\frac{u(1-u)}{\beta\sigma} - \frac{v}{\alpha\beta\sigma} \leq \frac{\alpha\beta\sigma + 1}{\alpha\beta^2\sigma^2} - \frac{w}{\alpha\beta\sigma},$$

where $w = u/(\beta\sigma) + v$. Since both u and v are nonnegative, we have $v(\cdot, 0) \leq w(\cdot, 0)$. Using the comparison theorem again, we have

$$0 < v(\cdot, t) \leq w(\cdot, t) < \alpha + \frac{1}{\beta\sigma},$$

for all time $t > 0$ if $0 < v(\cdot, 0) < \alpha + \frac{1}{\beta\sigma}$. From (21), one can deduce $\Delta t \leq 1$ for the bounds of the pre-computed interpolating points to be valid; hence, we have $\Delta t \leq 1/\sigma$ by scaling from v . Thus, the boundedness of both $\|u^*\|_\infty$ and $\|v^*\|_\infty$ is also valid.

Now we proceed the second formula of the method. Since

$$\begin{aligned} u_{ij}^{n+1} &= \mathcal{L}_h^u(\Delta t)u_{ij}^n \\ &= u_{ij}^* + \Delta t \frac{u_{i+1,j}^* + u_{i-1,j}^* + u_{i,j+1}^* + u_{i,j-1}^* - 4u_{ij}^*}{h^2} \\ &< u_{ij}^* + 4\Delta t \frac{1 - u_{ij}^*}{h^2} \end{aligned} \quad (22)$$

In order for the third line of (22) to be bounded by 1 for all $1 \leq i \leq N_x$ and $1 \leq j \leq N_y$, a time step restriction is $\Delta t \leq \min\{1, \sigma h^2/4\}$. In a similar manner, $\Delta t \leq \min\{1/\sigma, h^2/4\}$ holds in order to maintain the boundedness of v_{ij}^* for v_{ij}^{n+1} ; we take the latter.

Therefore, we have

$$\|u^{n+1}\|_\infty < 1, \quad \|v^{n+1}\|_\infty < \alpha + \frac{1}{\beta\sigma}.$$

This completes the proof.

For the next step, we provide the following lemmas.

Lemma 5 Assume that $\Delta t \leq 1/\sigma$. Then

$$\|\mathcal{N}_h^u(\Delta t)\tilde{U}\|_2 \leq e^{\Delta t}\|\tilde{U}\|_2, \quad \|\mathcal{N}_h^v(\Delta t)\tilde{V}\|_2 \leq e^{\Delta t}\|\tilde{V}\|_2,$$

for any $\tilde{U}, \tilde{V} \in \mathbb{R}^{N_x \times N_y}$ satisfying $\|\tilde{U}\|_\infty < 1$, and $\|\tilde{U}\|_\infty < \|\tilde{V}\|_\infty < \alpha + \frac{1}{\beta\sigma}$.

Proof This result is directly derived from Theorem 3.

Lemma 6 Assume that $\Delta t \leq \min\{1/\sigma, h^2/4\}$. Then

$$\|\mathcal{L}_h^u(\Delta t)\tilde{U}\|_2 \leq e^{\Delta t}\|\tilde{U}\|_2, \quad \|\mathcal{L}_h^v(\Delta t)\tilde{V}\|_2 \leq e^{\Delta t}\|\tilde{V}\|_2,$$

for any $\tilde{U}, \tilde{V} \in \mathbb{R}^{N_x \times N_y}$ satisfying $\|\tilde{U}\|_\infty < 1$, and $\|\tilde{U}\|_\infty < \|\tilde{V}\|_\infty < \alpha + \frac{1}{\beta\sigma}$.

Proof This result is also directly derived from Theorem 3.

Lemma 7 (Li et al. 2017) Assume that $u, v \in H^6(0, T; H^3(\Omega))$. Then we have

$$\begin{aligned} \|I^h \mathcal{N}^u(\Delta t)u - \mathcal{N}_h^u(\Delta t)I^h u\|_2 &\leq C_1 \Delta t^5, \\ \|I^h \mathcal{N}^v(\Delta t)v - \mathcal{N}_h^v(\Delta t)I^h v\|_2 &\leq C_2 \Delta t^5, \end{aligned}$$

$$\begin{aligned}\|I^h \mathcal{L}^u(\Delta t)u - \mathcal{L}_h^u(\Delta t)I^h u\|_2 &\leq C_3 \Delta t(\Delta t + h^2), \\ \|I^h \mathcal{L}^v(\Delta t)v - \mathcal{L}_h^v(\Delta t)I^h v\|_2 &\leq C_4 \Delta t(\Delta t + h^2),\end{aligned}$$

where C_1 , C_2 , C_3 , and C_4 are independent on Δt and h .

Proof The proof is similar that is given in Li et al. (2017). We omit the proof here for the sake of brevity.

Now we present the following convergence result. This result is also based on the framework in Li et al. (2017).

Theorem 4 We set $I^h u^0 = U^0 = u^0$ and $I^h v^0 = V^0 = v^0$, and let $\|u^0\|_\infty < 1$, $\|u^0\|_\infty < \|v^0\|_\infty < \alpha + \frac{1}{\beta\sigma}$. Assume that $\Delta t \leq \min\{1/\sigma, h^2/4\}$ and $u^0, v^0 \in H^k(\Omega)$ for some $k \geq 3$. Moreover, suppose that $u, v \in H^6(0, T; H^k(\Omega))$ are the exact solutions of the system (19). Let $U^{n+1} = I^h u((n+1)\Delta t)$, $V^{n+1} = I^h v((n+1)\Delta t)$ be the solutions assigned at all the grid points. Then there are C_1 and C_2 independent on Δt and h satisfying

$$\begin{aligned}\|U^{n+1} - u^{n+1}\|_2 &\leq C_1(\Delta t + h^2), \\ \|V^{n+1} - v^{n+1}\|_2 &\leq C_2(\Delta t + h^2).\end{aligned}$$

Proof For simplicity, we prove the case of u only. Assume that u^n is given. Now we apply the one-step exact solution operator $\mathcal{L}^u(\Delta t)\mathcal{N}^u(\Delta t)$ to \tilde{u}^n , denote it as $\tilde{U}^{n+1} = I^h \mathcal{L}^u(\Delta t)\mathcal{N}^u(\Delta t)\tilde{u}^n$. Then we have

$$\|U^{n+1} - u^{n+1}\|_2 \leq \|U^{n+1} - \tilde{U}^{n+1}\|_2 + \|\tilde{U}^{n+1} - u^{n+1}\|_2. \quad (23)$$

From (9), the first term on the right-hand side of (23) is the local one-step error; hence, it follows that

$$\|U^{n+1} - \tilde{U}^{n+1}\|_2 \leq C_1 \Delta t^2.$$

The second term on the right-hand side of (23) is

$$\begin{aligned}\|\tilde{U}^{n+1} - u^{n+1}\|_2 &\leq \|I^h \mathcal{L}^u(\Delta t)\mathcal{N}^u(\Delta t)\tilde{u}^n - \mathcal{L}_h^u(\Delta t)I^h \mathcal{N}^u(\Delta t)\tilde{u}^n\|_2 \\ &\quad + \|\mathcal{L}_h^u(\Delta t)I^h \mathcal{N}^u(\Delta t)\tilde{u}^n - \mathcal{L}_h^u(\Delta t)\mathcal{N}_h^u(\Delta t)u^n\|_2.\end{aligned} \quad (24)$$

Using Lemmas 6 and 7, then the right-hand side of (24) is bounded by

$$C_2 \Delta t(\Delta t + h^2) + e^{\Delta t} \|I^h \mathcal{N}^u(\Delta t)\tilde{u}^n - \mathcal{N}_h^u(\Delta t)u^n\|_2. \quad (25)$$

The second term in (25) is bounded by

$$e^{\Delta t} (\|I^h \mathcal{N}^u(\Delta t)\tilde{u}^n - \mathcal{N}_h^u(\Delta t)I^h \tilde{u}^n\|_2 + \|\mathcal{N}_h^u(\Delta t)I^h \tilde{u}^n - \mathcal{N}_h^u(\Delta t)u^n\|_2). \quad (26)$$

Using Lemmas 5 and 7, (26) is bounded by

$$e^{\Delta t} (C_3 \Delta t^5 + e^{\Delta t} \|I^h \tilde{u}^n - u^n\|_2).$$

Combining all above estimates yields

$$\begin{aligned}\|U^{n+1} - u^{n+1}\|_2 &\leq C(\Delta t^2 + \Delta t h^2 + \Delta t^5) + e^{2\Delta t} \|\tilde{U}^n - u^n\|_2 \\ &\leq (n+1)C(\Delta t^2 + \Delta t h^2) + e^{3T} \|\tilde{U}^0 - u^0\|_2 = C(\Delta t + h^2).\end{aligned}$$

The convergence of v can be analyzed in the same manner. This completes the proof.

We conclude this section with the following remark.

Remark 3 One might wonder the systems (12) and (19) have steady-state solutions with or without diffusion indeed. There are numerous existing studies (see Yi et al. 2009; Ko and Ryu 2006 and the references therein) have explained it well, we omit the linear stability analysis to the systems (12) and (19) and to the conventional Runge–Kutta method for those systems. Further note that the time step restrictions listed in Theorems 1 and 3 are not optimal; those can be improved.

4 Numerical experiments

In this section, we present the numerical simulation results to the models introduced in Sect. 3.

4.1 Linear stability

Based on the linear stabilities of the systems of equations (12) and (19) without diffusions (see Remark 3), we need to verify whether the numerical solution using interpolants indeed converges to the asymptotically stable equilibrium. For the sake of brevity, we consider the system (12) only. We split each equations from (12) into the two parts, and then the reaction system is as follows:

$$\frac{\partial u}{\partial t} = k_1 \left(v - \frac{uv}{1+v^2} \right), \quad \frac{\partial v}{\partial t} = k_2 - v - \frac{4uv}{1+v^2}. \quad (27)$$

Figure 3a shows the phase portrait of (27). Figure 3b, c illustrate numerical solutions using both the explicit fourth-order Runge–Kutta method and the interpolants with respect to u and v , respectively, over time until $t = 10$. In this test, we use $k_1 = 7$, $k_2 = 11$, $\Delta t = 0.1$, $N_t = 100$, $N_u = 150$, $N_v = 100$, $N_s = 10$, and the equilibrium node $(\bar{u}, \bar{v}) = (1 + 0.04k_2^2, 0.2k_2)$.

According to Fig. 3, (\bar{u}, \bar{v}) is indeed a numerically stable node. Moreover, the numerical solutions using interpolants fit well into the solutions using the Runge–Kutta method. Therefore, this gives a rationale for using the interpolating functions to derive the numerical solution of (2). From now on, we take the following stopping criterion for the pre-computing process, $tol < 10^{-5}$, where

$$tol = \max \left\{ \frac{\|u^{N_s-1} - u_{ref}\|_{2,\Omega_H}}{\|u_{ref}\|_{2,\Omega_H}}, \frac{\|v^{N_s-1} - v_{ref}\|_{2,\Omega_H}}{\|v_{ref}\|_{2,\Omega_H}} \right\}.$$

Note that u_{ref} and v_{ref} are reference solutions using a fine step $\Delta t_s/N_s^2$. We start with $N_s = 2$ and gradually increasing it until $tol < 10^{-5}$.

4.2 Convergence test

We observe the convergence rate of the proposed numerical scheme in this subsection. First we measure the convergence rate in time that we employ the periodic boundary condition to the model (12). Here, we use $N = N_x = N_y = 128$ in $[0, 10] \times [0, 10]$, $k_1 = 7$, $k_2 = 11$,

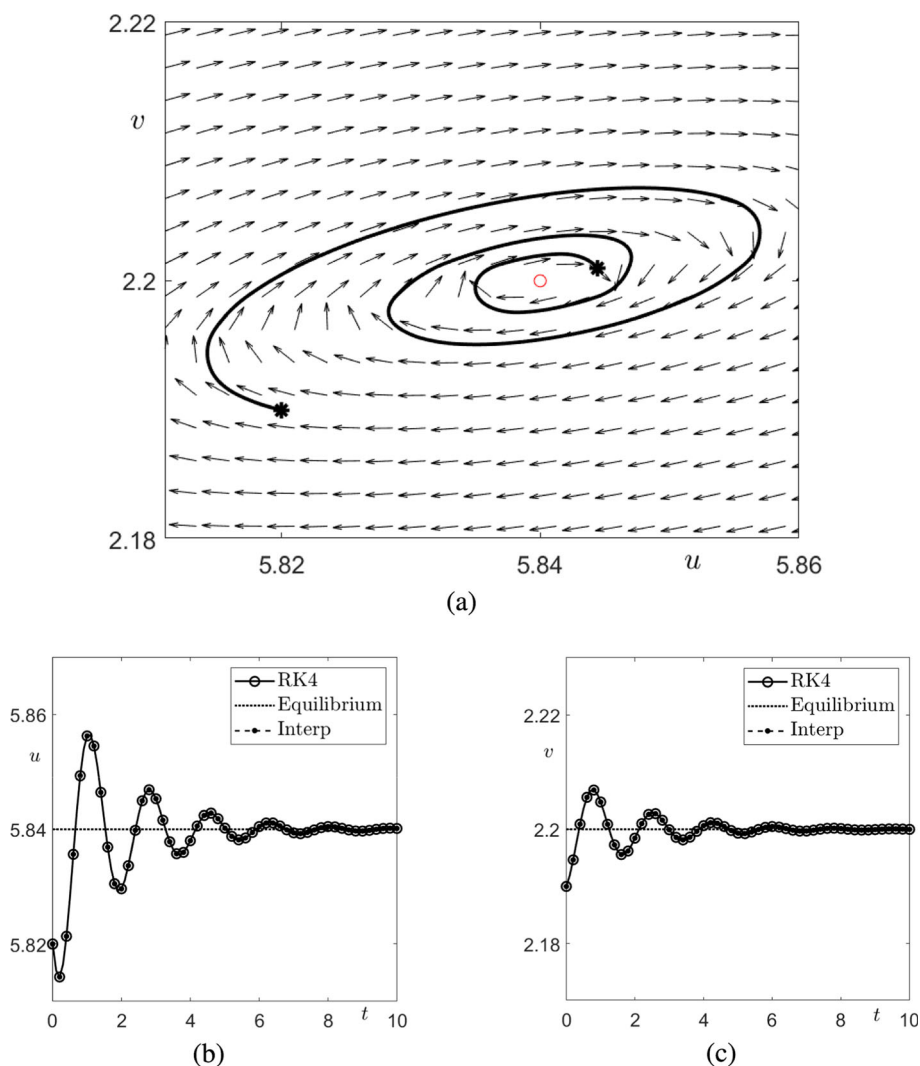


Fig. 3 **a** Phase portrait of (27). Here, we use the neighborhood values (5.82, 2.19) (solid line with star-shape marker) and (5.86, 2.22) (dotted line with circular-shape marker). **b**, **c** are the plots of numerical solutions with respect to u and v , respectively. Note that the interval between each marker is $2\Delta t$

$\delta = 0.04$, and $T = 1$. The following initial conditions are employed.

$$\begin{aligned} u(x, y, 0) &= \bar{u} + 0.1 \cos \frac{2\pi x}{10} \cos \frac{2\pi y}{10}, \\ v(x, y, 0) &= \bar{v} + 0.1 \cos \frac{2\pi x}{10} \cos \frac{2\pi y}{10}. \end{aligned} \quad (28)$$

Table 1 Rate of convergence in time to the proposed scheme. Note that we omit the second place of $e_w^t(\cdot, \cdot)$ for convenience below

| cases | $e_w^t(T/64, \cdot)$ | rate | $e_w^t(T/128, \cdot)$ | rate | $e_w^t(T/256, \cdot)$ | rate | $e_w^t(T/512, \cdot)$ |
|---------|----------------------|--------|-----------------------|--------|-----------------------|--------|-----------------------|
| $w = u$ | 6.677e-6 | 0.9973 | 3.345e-6 | 0.9986 | 1.674e-6 | 0.9994 | 8.373e-7 |
| $w = v$ | 8.741e-6 | 0.9717 | 4.457e-6 | 0.9861 | 2.250e-6 | 0.9931 | 1.130e-6 |

Furthermore, we define a relative error e_w^t between two numerical solutions using different time steps as

$$e_w^t(\Delta t_1, \Delta t_2) = \frac{\|w^{T, \Delta t_1} - w^{T, \Delta t_2}\|_2}{\|w^{T, \Delta t_1}\|_2} \quad \text{for } \Delta t_1 > \Delta t_2,$$

where $w^{T, \Delta t}$ implies that the numerical solution at $t = T$ with the time step Δt . Then we can define the rate of convergence as

$$\text{rate} = \log_2 \frac{e_w^t(\Delta t, \Delta t/2)}{e_w^t(\Delta t/2, \Delta t/4)}, \quad (29)$$

The time step Δt begins with $\Delta t = T/64$ and decreases by half. The final value is $\Delta t = T/1024$. Table 1 shows the rate of convergence in time of our method with the periodic boundary condition in the system (12).

According to Table 1, we verify that our method is of first-order in time. This coincides the fact (10) in Remark 1.

Now we verify the convergence rate in space. Since the initial conditions (28) are sufficiently smooth, we expect an exponential decay in the space error based on the result of Theorem 2. In order to measure the spectral accuracy in space, we consider the following relative error e_w^{per} between coarse and reference grid solutions as

$$e_w^{per}(N, N_{ref}) = \left(\frac{\sum_{1 \leq i, j \leq N} \left(w_{\frac{N_{ref}}{N}i, \frac{N_{ref}}{N}j}^{T, N_{ref}} - w_{ij}^{T, N} \right)^2 \right)^{1/2}}{\sum_{1 \leq i, j \leq N} \left(w_{\frac{N_{ref}}{N}i, \frac{N_{ref}}{N}j}^{T, N_{ref}} \right)^2} \right)^{1/2},$$

where $w^{T, N_{ref}}$ is the reference grid solution, i.e., the finest grid solution, and $w^{T, N}$ is a relatively coarse grid solution. This error is well-defined since the collocation points in the frequency space are exactly same whenever the wave numbers are same. Figure 4 depicts the rate of convergence to our method is of exponential decay indeed.

Here, we set $N_{ref} = 1024$, $N = 32, 64, 128, 256, 512$, $\Delta t = 10^{-3}$, and $T = 10^{-1}$.

Finally, we verify the convergence rate in space with the homogeneous boundary condition, i.e., when using the explicit diffusion solver. For the sake of brevity, we use the system (12) with the homogeneous boundary condition; though it was not covered theoretically in Sect. 3, applying the solver (8) to (12) poses no problem. Since the expected convergence rate is $\mathcal{O}(\Delta t + h^2)$, if we take $\Delta t = 0.1h^2$, and then the rate becomes $\mathcal{O}(h^2)$. We define a relative error e_w^{hom} between two numerical solutions using different space steps N and $2N$ as

$$e_w^{hom}(N, 2N) = \frac{\|w^{T, N} - \tilde{w}^{T, 2N}\|_2}{\|w^{T, N}\|_2},$$

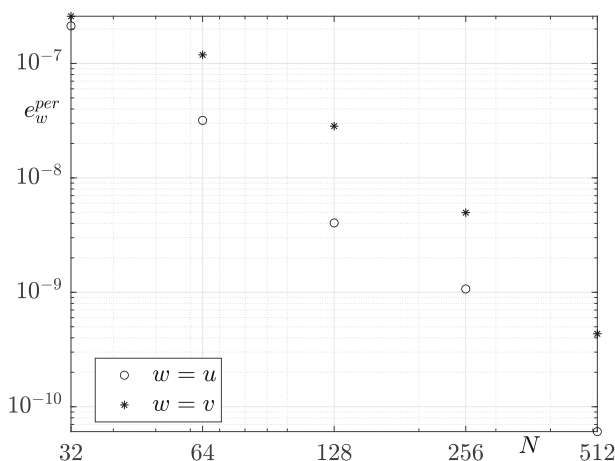


Fig. 4 Rate of convergence in space to the proposed scheme with the periodic boundary condition. Note that this is a log-log plot

Table 2 Rate of convergence in space to the proposed scheme with the homogeneous boundary condition. Note that we omit the second place of $e_w^{hom}(\cdot, \cdot)$ for convenience below

| Cases | $e_w^{hom}(32, \cdot)$ | Rate | $e_w^{hom}(64, \cdot)$ | Rate | $e_w^{hom}(128, \cdot)$ | Rate | $e_w^{hom}(256, \cdot)$ |
|---------|------------------------|--------|------------------------|--------|-------------------------|--------|-------------------------|
| $w = u$ | 9.643e-6 | 1.9850 | 2.436e-6 | 1.9980 | 6.099e-7 | 1.9961 | 1.529e-7 |
| $w = v$ | 4.368e-5 | 1.9888 | 1.100e-5 | 1.9974 | 2.756e-6 | 1.9987 | 6.897e-7 |

where $w^{T,N}$ represents the numerical solution at $t = T$ with $N \times N$ grid points, and $\tilde{w}^{T,2N}$ is defined as

$$\tilde{w}_{ij}^{T,2N} = \frac{w_{2i-1,2j-1}^{T,2N} + w_{2i-1,2j}^{T,2N} + w_{2i,2j-1}^{T,2N} + w_{2i,2j}^{T,2N}}{4},$$

for all $1 \leq i, j \leq N$. The following table shows that our proposed method with the homogeneous boundary condition is of second-order in space indeed. Here, we use $N = 32, 64, 128, 256$, $\Delta t = 0.1h^2$, $T = h^2$, and measure the rate in the sense of (29).

According to Fig. 4 and Table 2, we conclude that our method has advantages in the sense of spectral accuracy and relaxed time step size compared to the fully explicit and conventional semi-implicit methods.

4.3 Pattern formation

We provide several patterns induced by the models (12) and (19) in this subsection.

4.3.1 Stripes and spots

Figure 5 shows the temporal evolution of the system (Lengyel and Epstein 1992) in 2D for different values of k_1 and δ . The system is solved in $(x, y) \in [0, 10] \times [0, 10]$, $k_2 = 11$, $N_x = 100$, $N_y = 100$, $h = 0.1$, and $\Delta t = 0.001$. Here, we use the pre-computing parameters

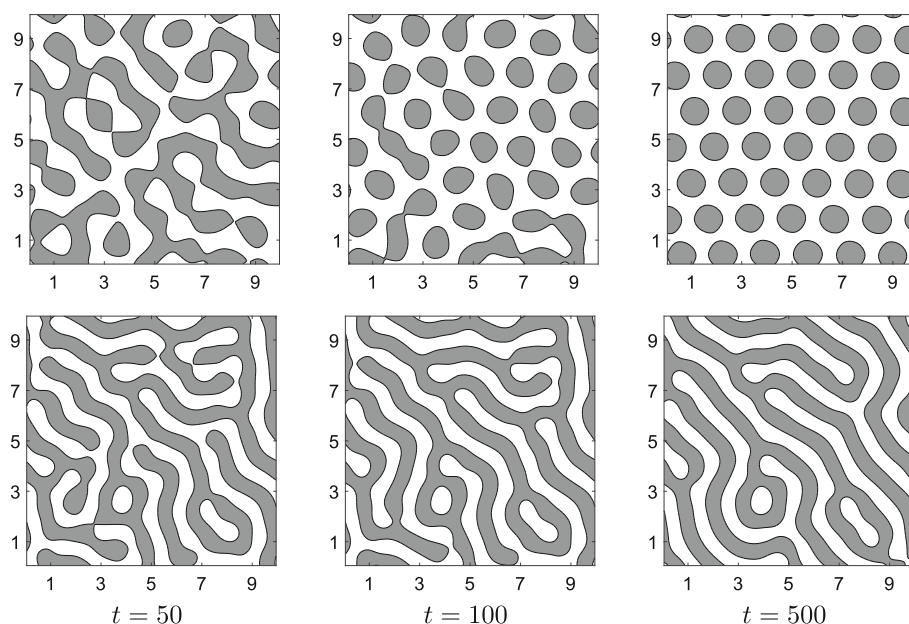


Fig. 5 Temporal evolution of the Lengyel–Epstein model with $k_2 = 11$. In first row, $\delta = 0.04$ and $k_1 = 7$ are used. In second row, $\delta = 0.02$ and $k_1 = 9$ are used. The final times for each pattern is $t = 50$, $t = 100$, and $t = 500$ from left to right

$N_u = 150$, $N_v = 150$, and $N_s = 200$. Initial conditions are given as follows:

$$\begin{aligned} u(x, y, 0) &= \bar{u} + 0.2\text{rand}(x, y), \\ v(x, y, 0) &= \bar{v} + 0.2\text{rand}(x, y), \end{aligned} \quad (30)$$

where $\bar{u} = 1 + 0.04k_2^2$, $\bar{v} = 0.2k_2$, and $\text{rand}(x, y)$ implies a random value between -1 and 1 . We employ the periodic boundary condition.

We provide the L^2 -stability result numerically. Figure 6 shows a consecutive error over time until $t = 500$. The relative consecutive error is defined as follow:

$$\text{consecutive error} = \frac{\|w^{n+1} - w^n\|_2}{\|w^n\|_2}.$$

All the parameters are not changed those in the previous test.

Next, we show the specific effect of parameter δ in pattern formation. We use three values of $\delta = 0.01$, 0.03 , and 0.04 , with remaining parameters fixed. The results of using different δ are shown in Fig. 7. As δ changes from 0.01 to 0.03 and 0.04 , we can find the transition from concave spots pattern to stripes, and back to convex spots pattern.

4.3.2 Spiral traveling waves

We apply the model (Sherratt et al. 2002) to generate periodic traveling wave solutions of an area containing a landscape obstacle listed in Yun et al. (2015), which is depicted in Fig. 8.

The following values are assigned to parameters, $\alpha = 1.8$, $\beta = 1.2$, $\gamma = 4.9$, and $\sigma = 2.5$. We perform the pre-computing process to obtain interpolating points for nonlinear terms of

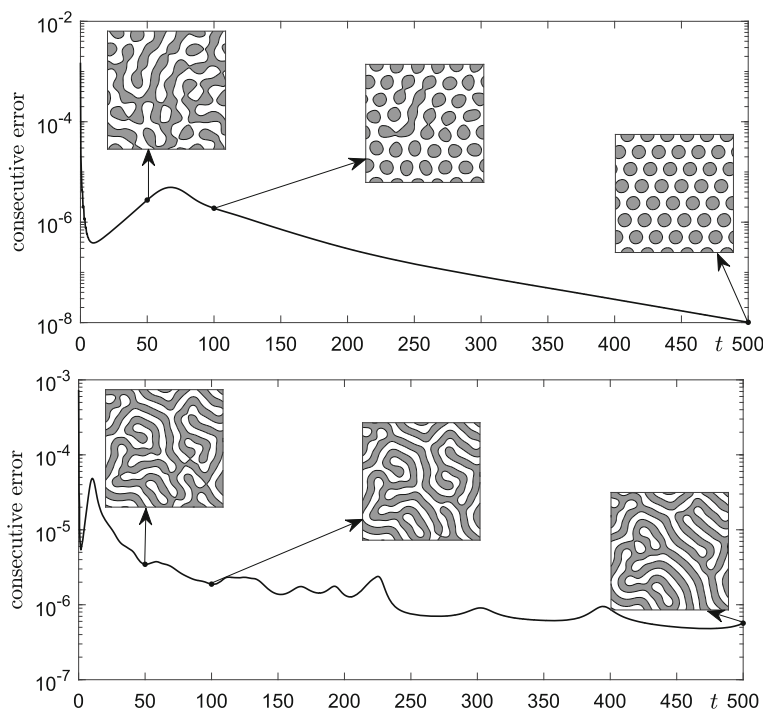


Fig. 6 The consecutive error with $k_2 = 11$. In first row, $\delta = 0.04$ and $k_1 = 7$ are used. In second row, $\delta = 0.02$ and $k_1 = 9$ are used

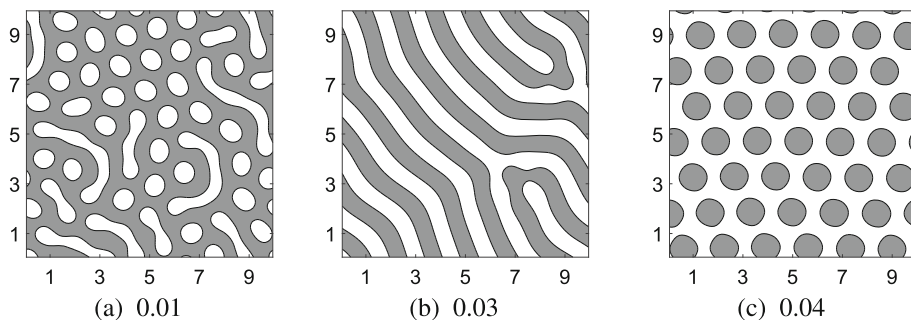


Fig. 7 Pattern formation using different values of $\delta = 0.01, 0.03, 0.04$ and $k_1 = 7$ at $t = 500$

the predator–prey model with $N_u = 50$, $N_v = 50$, and $N_s = 50$. The following initial condition is given:

$$\begin{aligned} u(x, y, 0) &= I_{xy}(1.1\bar{u} + 0.05\text{rand}(x, y)), \\ v(x, y, 0) &= I_{xy}(1.1\bar{v} + 0.05\text{rand}(x, y)), \end{aligned} \quad (31)$$

where I_{xy} is an indicator function satisfying $I_{xy} = 0$ if (x, y) is in obstacle; $I_{xy} = 1$ otherwise where $(x, y) \in [0, 512] \times [0, 512]$. Figure 9 shows the traveling wave solutions nearby an obstacle, which is the landscape. We use $\Delta t = 1/\sigma$, $N_x = N_y = 512$, and $h = 1$.

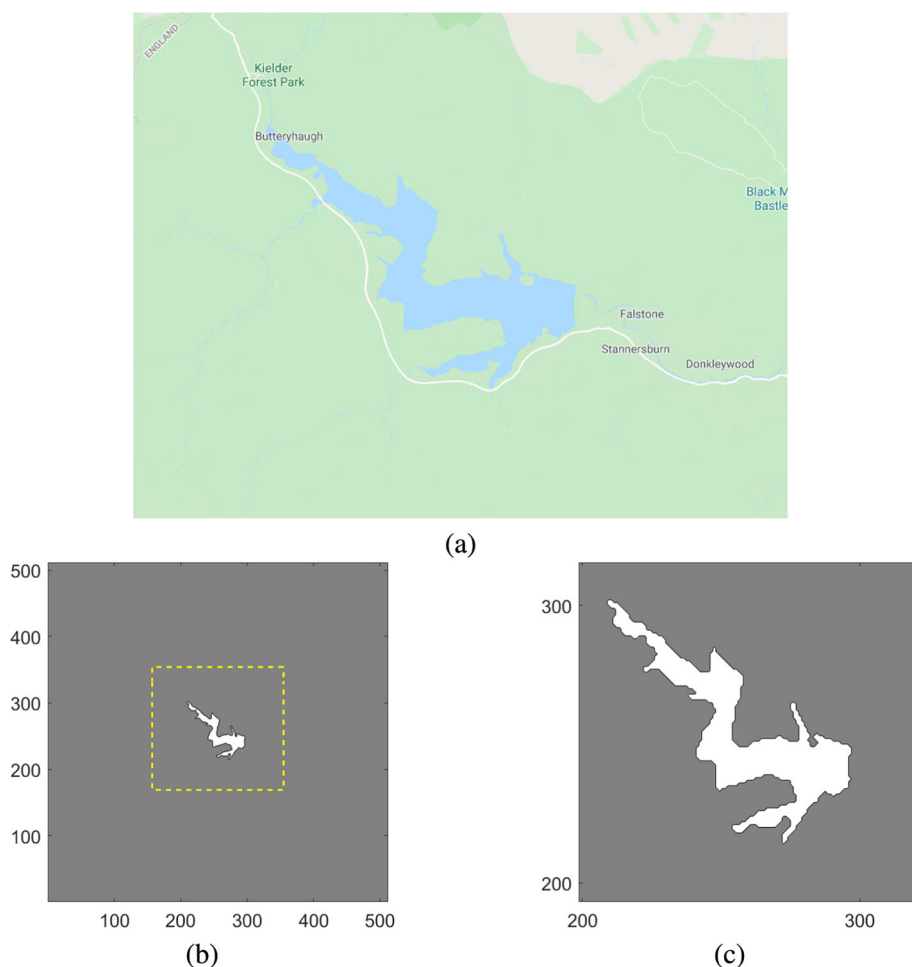


Fig. 8 **a** Photograph of Kielder Water provided by Google Maps. **b** Geometric landscape feature presented in Yun et al. (2015), which is an obstacle in domain. **c** Close up view of yellow boxed region

4.4 Performance of computing time

In this section, we compare the total computing time of numerical methods using our proposed method with those of references using their scheme. First, let us consider the comparison of the computing time for the Lengyel–Epstein model. In Jeong et al. (2017), the numerical solution of (2) is obtained by the explicit Euler method which has a severe time step restriction, whereas the proposed method in this paper is relatively free from the time step restriction. For comparison, we ran the test until final time $t = 2000$ for both methods. The referenced method showed unstable results when $\Delta t = 0.01$, whereas the proposed scheme showed stable results. For the reference method, $\Delta t = 0.001$ is used for the test and any other parameters are not changed those in Jeong et al. (2017).

Table 3 contains the computing time and used time step for both the reference method and our proposed scheme at the final time $t = 2000$ when $\delta = 0.04$ and $k_1 = 7$. As shown in

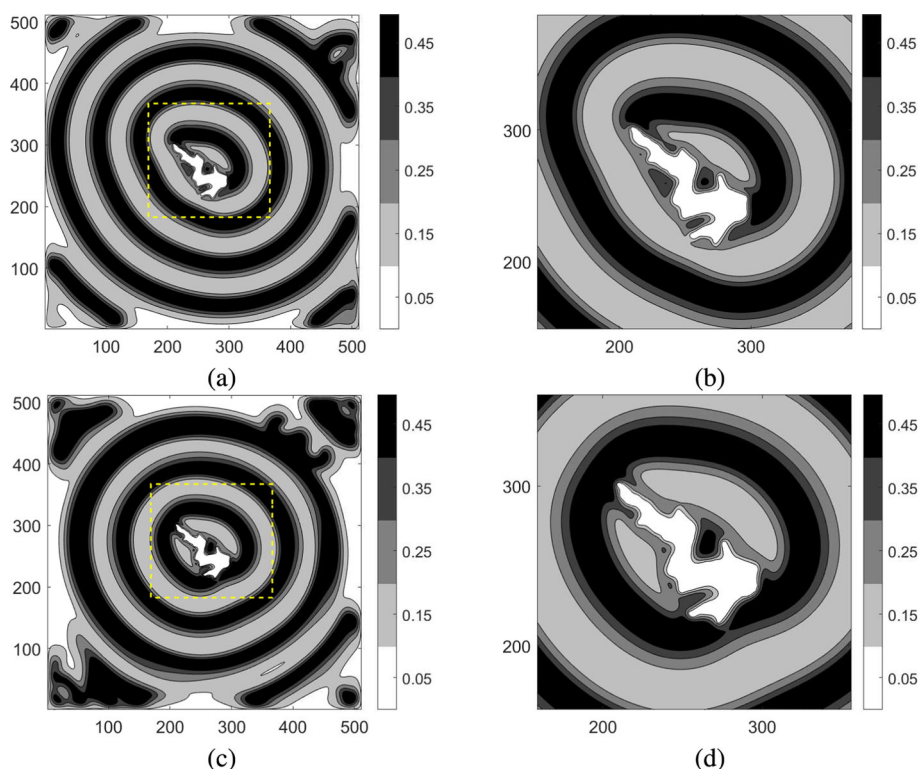


Fig. 9 **a** Traveling wave solution around the landscape obstacle at $t = 7000$. **b** Close up view of yellow boxed region in **a**. **c** Traveling wave solution around the landscape obstacle at $t = 10000$. **d** Close up view of yellow boxed region in **c**

Table 3 Computing time performance for the Lengyel–Epstein model between our proposed scheme and the reference method

| | Proposed scheme | Reference method |
|------------------|-----------------|------------------|
| Δt | 0.01 | 0.001 |
| Elapsed time (s) | 218.11 | 281.80 |

Table 4 Computing time performance for the predator–prey model between our proposed scheme and the reference method

| | Proposed scheme | Reference method |
|------------------|-----------------|------------------|
| Δt | 0.25 | 0.25 |
| Elapsed time (s) | 707.21 | 6553.41 |

Table 3, our proposed scheme achieves a quite faster computation than the reference method by using a larger time step size.

For the next step, we compare the elapsed time between our method and the splitting-based multigrid solver employed in Yun et al. (2015) with the same time step $\Delta t = 0.25$. Any other parameters are fixed as listed in Yun et al. (2015). Table 4 shows the CPU time performance between two schemes at the final time $t = 7000$.

According to Table 4, our proposed method is much faster than the reference method. This indicates that our approach offers faster performance compared to a kind of implicit solver.

5 Discussions

We aim to discuss several points of consideration regarding the content presented so far in this section. Let us start with the reason for using the explicit fourth order Runge–Kutta method in the pre-computing process. As mentioned in Remark 1, the local error is $\mathcal{O}(\Delta t^2)$, which implies that using a high-order scheme beyond the second order is not meaningful in reducing the discretized error. However, the pre-computed solution is utilized at every step in the time integration to compute the next intermediate solution in the main loop. Although our proposed method is classified as a hybrid scheme, it essentially operates like a linear method due to the closed-form nature of the linear interpolation method. It is important to note that the pre-computed solution is not a one-step solution. This means that another type of error in the solution, such as a round-off error, must also be considered during the pre-computing process. Therefore, we have considered reducing the number of pre-iterations, N_s , in the pre-computing process, and consequently chosen the conventional Runge–Kutta method over the forward Euler scheme. It is worth noting that since $\Delta t/N_s$ is the one-step size in the pre-computing process, a sufficiently small time step is already required, thus excluding implicit solvers from our options. Additionally, although the models discussed above are not highly nonlinear, our approach can be easily extended to an adaptive Runge–Kutta method in cases where regarding models are more stiff than the above models.

Next, we address the reasons for using a linear interpolating method and discuss the extension of it. The reason for using bilinear interpolation as a nonlinear propagator in our proposed method is due to the ease of obtaining the boundedness of the solution. However, there is a drawback of the currently selected method that Ω_H , which is the discretized linearly stable region for u and v in the pre-computing process, requires a relatively large number of mesh grids. For a highly stiff nonlinear problem, the linear interpolation requires a finer grid compared to other methods to achieve sufficient accuracy. This also implies an increase in the time required to locate the specific cell in Ω_H where u_{ij}^n and v_{ij}^n should be positioned for each step when applying the nonlinear propagator in the main loop; in other words, it affects the elapsed time. To advance this, we can consider the non-uniform mesh refinement or the latest interpolating methods that can reduce the resolution of Ω_H . Various interpolating methods applicable to different reaction-diffusion systems have been actively developed until recently (Roul 2020; Roul and Goura 2023).

Finally, we discuss the setting of initial conditions and the instabilities that might emerge from discretization. As mentioned above, the patterns are generated through the instabilities driven by diffusion in the linearly stable region with the unique steady-state (in fact, asymptotically stable) solution (w^*, z^*) . Due to the comparison arguments presented in Smoller (2012), it is possible to obtain the *all* time bound $|w(\cdot, t) - w^*| \leq |z(\cdot, t) - z^*|$ once $|w(\cdot, 0) - w^*| \leq |z(\cdot, 0) - z^*|$ has been established. This fact provides a rationale that, even if the numerical solution at a specific time falls outside the stable region, the boundedness at the discrete level can be guaranteed by setting the initial values closer to the asymptotically stable equilibrium. This is the reason why we set the initial conditions as described in (30) and (31).

6 Conclusions

In this paper, we present the result of alleviating the time step restriction when solving the system of reaction-diffusion equations through the pre-iterations process and achieve the fast

computation to the whole reaction-diffusion system. When solving the system of the ordinary differential equations, the results using interpolants and the fourth-order Runge–Kutta method are not significantly different. We provide the stability and convergence results for Lengyel–Epstein and predator–prey models both theoretical and numerical ways, and both results are in good agreements. Numerical simulations are conducted and the results imply that our proposed method brings out similar patterns as well as the patterns derived in the references. One of the advantages of the proposed method, as demonstrated by the comparison of the computing time performance with explicit or implicit solvers, is that our method can provide the numerical solutions of similar qualities more faster. For future research, we aim to extend our method to models that form patterns differently from conventional reaction-diffusion models, such as time-fractional diffusion or doubly nonlocal models (Roul et al. 2023, 2022; Gal 2018).

Acknowledgements The first author (S. Yoon) was supported by the National Research Foundation of Korea (NRF) grant funded by the Ministry of Science and ICT of Korea (MSIT) (No. 2019R1A6A1A11051177) and by Basic Science Research Program through the National Research Foundation of Korea (NRF) funded by the Ministry of Education (MOE) (No. 2022R111A1A01073661). The author (C. Lee) was supported by the National Research Foundation of Korea (NRF) grant funded by the Korea government (MSIT) (No. 2022R1C1C2003896). The corresponding author (J.S. Kim) was supported by the National Research Foundation of Korea (NRF) grant funded by the Korea government (MSIT) (No. 2022R1A2C1003844). The authors extend their thanks to the reviewers for the valuable and constructive input they provided during the revision of the article.

Data availability The datasets generated and/or analyzed during the current study are available from the corresponding author upon reasonable request.

Declarations

Conflict of interest All the authors declare that they have no conflict of interest.

References

- Barrio R, Varea C, Aragón J, Maini P (1999) A two-dimensional numerical study of spatial pattern formation in interacting Turing systems. *Bull Math Biol* 61(3):483–505
- Bisi M, Travaglini R (2022) Reaction-diffusion equations derived from kinetic models and their Turing instability. *Commun Math Sci* 20(3):763–801
- Dunbar SR (1986) Traveling waves in diffusive predator-prey equations: periodic orbits and point-to-periodic heteroclinic orbits. *SIAM J Appl Math* 46(6):1057–1078
- Ermentrout B (1991) Stripes or spots? Nonlinear effects in bifurcation of reaction-diffusion equations on the square. *Proc R Soc Lond Ser A Math Phys Sci* 434(1891):413–417
- Fuselier EJ, Wright GB (2013) A high-order kernel method for diffusion and reaction-diffusion equations on surfaces. *J Sci Comput* 56(3):535–565
- Gal CG (2018) Doubly nonlocal Cahn–Hilliard equations. *Annales de l’Institut Henri Poincaré C, Analyse non linéaire* 35(2):357–392
- Greenberg J, Hassard B, Hastings S (1978) Pattern formation and periodic structures in systems modeled by reaction-diffusion equations. *Bull Am Math Soc* 84(6):1296–1327
- Jeong D, Li Y, Choi Y, Yoo M, Kang D, Park J, Choi J, Kim J (2017) Numerical simulation of the zebra pattern formation on a three-dimensional model. *Phys A Stat Mech Appl* 475:106–116
- Jia H, Li K (2011) A third accurate operator splitting method. *Math Comput Model* 53(1–2):387–396
- Ko W, Ryu K (2006) Qualitative analysis of a predator-prey model with Holling type II functional response incorporating a prey refuge. *J Differ Equ* 231(2):534–550
- Kondo S, Miura T (2010) Reaction-diffusion model as a framework for understanding biological pattern formation. *Science* 329(5999):1616–1620

- Lengyel I, Epstein IR (1992) A chemical approach to designing Turing patterns in reaction-diffusion systems. *Proc Natl Acad Sci* 89(9):3977–3979
- Li X, Qiao Z, Zhang H (2017) Convergence of a fast explicit operator splitting method for the epitaxial growth model with slope selection. *SIAM J Numer Anal* 55(1):265–285
- Li D, Quan C, Xu J (2022) Stability and convergence of Strang splitting. Part I: scalar Allen–Cahn equation. *J Comput Phys* 458:111087
- Lou Y, Ni W-M (1996) Diffusion, self-diffusion and cross-diffusion. *J Differ Equ* 131(1):79–131
- Lyons MJ, Harrison LG (1992) Stripe selection: an intrinsic property of some pattern-forming models with nonlinear dynamics. *Dev Dyn* 195(3):201–215
- Othmer H, Pate E (1980) Scale-invariance in reaction-diffusion models of spatial pattern formation. *Proc Natl Acad Sci* 77(7):4180–4184
- Roul P (2020) A fourth-order non-uniform mesh optimal B-spline collocation method for solving a strongly nonlinear singular boundary value problem describing electrohydrodynamic flow of a fluid. *Appl Numer Math* 153:558–574
- Roul P, Goura VP (2019) B-spline collocation methods and their convergence for a class of nonlinear derivative dependent singular boundary value problems. *Appl Math Comput* 341:428–450
- Roul P, Goura VP (2022) A superconvergent B-spline technique for second order nonlinear boundary value problems. *Appl Math Comput* 414:126615
- Roul P, Goura VP (2023) An efficient numerical scheme and its stability analysis for a time-fractional reaction diffusion model. *J Comput Appl Math* 422:114918
- Roul P, Kumari T, Rohil V (2022) A computational technique for solving the time-fractional Fokker–Planck equation. *Math Methods Appl Sci* 45(16):9736–9752
- Roul P, Goura VP, Cavoretto R (2023) A numerical technique based on B-spline for a class of time-fractional diffusion equation. *Numer Methods Partial Differ Equ* 39(1):45–64
- Sherratt J, Lambin X, Thomas C, Sherratt T (2002) Generation of periodic waves by landscape features in cyclic predator-prey systems. *Proc R Soc Lond Ser B Biol Sci* 269(1489):327–334
- Smoller J (2012) Shock waves and reaction-diffusion equations, vol 258. Springer, Berlin
- Trotter HF (1959) On the product of semi-groups of operators. *Proc Am Math Soc* 10(4):545–551
- Turing AM (1990) The chemical basis of morphogenesis. *Bull Math Biol* 52(1/2):153–197
- Yi F, Wei J, Shi J (2009) Global asymptotical behavior of the Lengyel–Epstein reaction-diffusion system. *Appl Math Lett* 22(1):52–55
- Yun A, Shin J, Li Y, Lee S, Kim J (2015) Numerical study of periodic traveling wave solutions for the predator-prey model with landscape features. *Int J Bifurc Chaos* 25(09):1550117
- Zhu J, Zhang Y-T, Newman SA, Alber M (2009) Application of discontinuous Galerkin methods for reaction-diffusion systems in developmental biology. *J Sci Comput* 40:391–418

Publisher's Note Springer Nature remains neutral with regard to jurisdictional claims in published maps and institutional affiliations.

Springer Nature or its licensor (e.g. a society or other partner) holds exclusive rights to this article under a publishing agreement with the author(s) or other rightsholder(s); author self-archiving of the accepted manuscript version of this article is solely governed by the terms of such publishing agreement and applicable law.